2023 IEEE/ASME International Conference on Advanced Intelligent Mechatronics (AIM)
June 28-30, 2023. Seattle, Washington, USA

A high-bandwidth closed-loop MEMS force sensor with system dynamics adjustment

Diyako Dadkhah
Erik Jonsson School of Engineering and Computer Science,
The University of Texas at Dallas,
Richardson, TX, 75080 USA
diyako.dadkhah@utdallas.edu

S. O. Reza Moheimani*
Erik Jonsson School of Engineering and Computer Science,
The University of Texas at Dallas,
Richardson, TX, 75080 USA
reza.moheimani@utdallas.edu

***Abstract*—This paper describes a high-bandwidth control system design procedure for a MEMS force sensor equipped with an adjustable stiffness mechanism. When the force sensor comes into contact with a sample that has a stiffness at least comparable to its longitudinal stiffness, the resulting mechanical contact causes the system to become stiffer. This change in stiffness can be seen through the rising resonance frequency and falling dc-gain. In order to maintain closed-loop stability of the system after contact, it is necessary to tune the controller parameters since they are originally designed for the nominal system. By implementing a control system that combines an inner damping loop with a tracking loop together with adaptive algorithms to re-tune the controllers after contact, we were able to obtain satisfactory closed-loop performance. Also, the stiffness adjustment mechanism provides additional means of tuning the system dynamics. The numerical and experimental results demonstrate that these control approaches significantly increase the force tracking bandwidth.**

***Index Terms*—Microelectromechanical systems, MEMS force sensor, control of MEMS, vibration control.**

I. Introduction

Force measurements of micro- and nano-scale objects is an effective way of understanding their material properties. Developing high-precision force sensors that can measure dynamic forces over a wide frequency range, can lead to the development of innovative approaches for the characterization of various samples and technologies. Numerous techniques have been employed for force measurement. In [1], laser traps are used for conventional cellular force measurement. The challenge with this technique is that using a high intensity laser close to the UV spectrum increases the risk of damaging the sample. Applications of MEMS-based pressure sensor is addressed in [2]. However, using miniaturized silicon diaphragm devices smaller than a certain size will lead to a number of technical challenges as described in [3]. Reference [4] presents a piezoresistive force sensor array to measure cell vibration caused by ultrasound. In [5], a multi-axis capacitive cellular force sensor is used for force measurement on multiple axes.

Atomic force microscope (AFM) probes have also been employed as force sensors by measuring the interaction between the cantilever tip and a surface [6]. Estimation of rupture forces for the characterization of single molecular interactions [7], nanomechanical mapping of nanocomposites using force-deformation curves [8], measuring hydrodynamic force acting on the cantilever [9], and stiffness calibration of the AFM cantilever through dissipated energy method [10] are examples of this approach for force sensing. However, there are still several gaps in prior methodologies, resulting in limitations in the force measuring range with high resolution in micro and nano newtons. Design inflexibility, low measurement range, and limited degrees of freedom are some of these challenges.

Microelectromechanical systems (MEMS) technology has been used successfully to obtain accurate force measurements. MEMS devices are compact in size [11], power efficient, and remarkably functional [12]. Measuring stiffness of microcantilevers [13], characterization of nano-scale thin films in SEM and TEM [14], biological uses at cellular and organism levels [15], development of multifunctional surgical instruments [16], and manipulating micromechanical elements [17] are among practical applications of these force sensors.

Force sensing with MEMS is often accomplished by translating the applied force to a displacement using a mechanical structure. Different types of sensors, depending on the application, can be used to measure and interpret this displacement. Having a motion sensor allows us to conduct the experiments in closed loop rather than in open loop. In the open-loop case, the input force can be determined from the measured displacement and longitudinal stiffness of the flexures using Newton's law. In cases when the sample is relatively stiff, the nonlinearities caused by the deflection of mechanical flexures can be problematic, resulting in inaccurate measurements. In this situation, the closed-loop scenario becomes a viable option, where the output signal of the sensor is used in a feedback loop to keep the force sensor at the null position. Since the control signal maintains the system at its initial position, we can reasonably conclude that the applied actuation signal is balancing the external force, and thus their magnitudes are equal. Increasing the system's robustness, having the ability to measure dynamic and large-amplitude forces with better resolution, and ensuring the stability of the system are among the advantages of using feedback loops in force tracking.

The stiffness of the MEMS force sensor relative to the sample's is critical in the characterisation of different materials. When using a stiff force sensor, the sample may experience significant deformation before the contact force becomes quantifiable. This may lower measurement accuracy

and raise the risk of damaging the sample. Developing a force sensor more compliant than the sample may be a solution. Several constraints, however, impose limits on such a system, as force sensor stiffness has a direct impact on the measurement accuracy of the force sensor. Furthermore, if the sample stiffness is comparable to or greater than the stiffness of the force sensor, system dynamics will change. Such variations are generally undesirable as the controller parameters are originally determined based on the system's initial dynamics. As a result, the closed-loop system may behave differently, generating unexpected results. Being able to mechanically adjust stiffness of the force sensor makes the system usable under different situations. Several methods have been examined for this purpose. The method of varying gap is employed in [18], where seven different comb finger designs are implemented in micromechanical resonators to achieve a resonance shift. In [19], electrostatic comb fingers are used for stiffness tuning, where the fingers of the stationary and moving parts generate a positive or negative force depending on their arrangement. Another stiffness adjustment mechanism was introduced in [20] for an AFM cantilever, where two additional beams can be attached to the main compliant structure by applying a voltage to the plates of two electrostatic actuators, resulting in an increase in the overall stiffness of the system.

In this paper, we employ a MEMS force sensor with an on-chip stiffness-adjusting mechanism based on parallel plates reported in [21]. Using this stiffness adjustment technique, we are able to tune the system dynamics based on the current condition and, consequently, increase the force measurement bandwidth of the force sensor significantly. The device is operated in closed-loop, and its performance is assessed by applying various external forces using an AFM probe presented in [22]. To achieve the requisite stability and better tracking, we tune a resonant controller in addition to what was reported in [21] . This approach efficiently dampens oscillatory dynamics, and enables us to achieve a wider bandwidth both in zero-displacement and force tracking. We were able to increase the force-tracking bandwidth even more by modifying the loop gain online along with using the stiffness-adjustment mechanism.

II. MEMS FORCE SENSOR

As shown in Fig. 1, the device consists of a shuttle beam in the center that interacts with the sample via a probe at the end. The device is made up of two sets of comb-drives that, depending on the voltage applied, can attract or repulse each other, enabling bi-directional movement. This configuration leads the comb-drives to behave linearly. A non-contact electrothermal displacement sensor is integrated within the device due to its simple structure and simplicity in the fabrication process, since the heaters and the stage are in the same plane. The heaters have small footprints and do not add a large mechanical stiffness to the system. When operated under a bias voltage of 5 V, the electrothermal sensor shows a sensitivity of 1.9 μm/V. Although increasing the bias voltage makes the sensor more sensitive to displacements, doing so excessively can cause the sensor to burn. Therefore, finding a suitable and feasible bias voltage is an essential factor in the force sensing process. A displacement amplification mechanism is also employed to expand the displacement range, thereby increasing the force sensor's sensitivity. In addition, a parallel-plate stiffness-adjustment mechanism is utilized and will be covered in section II-B. The full characterization of the MEMS force sensor in time and frequency domains is reported in [21].

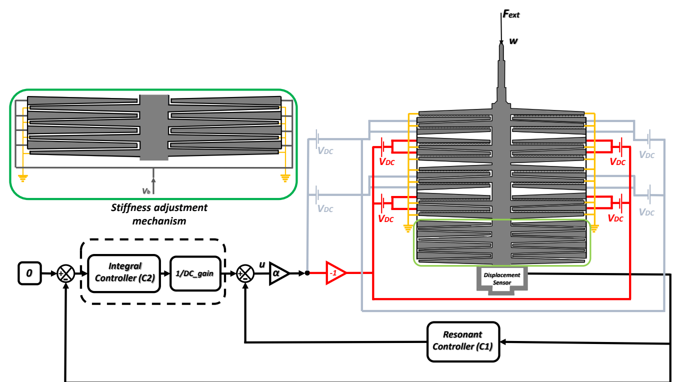

Fig. 1: Force sensor schematic and the block-diagram of the feedback control loop

A. System transfer function and estimation

The frequency response presented in Fig. 2 reveals the system dynamics, wherein only the result for zero stiffness adjustment voltage is shown. The second-order model:

$$G(s) = \frac{1.484e08}{s^2 + 209.4s + 4.287e07} \quad (1)$$

shown by the blue dashed curve in Fig. 2 captures the dynamics of the force sensor with good accuracy. This transfer function G(s) will be used as the nominal system model, and the analysis of the control in section III will be applied to this model.

B. Stiffness adjustment mechanism

A parallel-plate capacitive structure is used to realize the stiffness-adjustment part that reduces the structure's added mass and hence increases the dc-gain of the system along with decreasing the resonant frequency of the system [21]. Frequency responses of the system are shown in Fig. 3 for various V_b voltages. By increasing the stiffness adjustment voltage form 0V to 50V, the resonant frequency is reduced from 1050 Hz to 592 Hz and the dc-gain is raised by 9.4 dB. This can be interpreted as a threefold decrease in the stiffness indicating the capability of tuning the device's stiffness using the stiffness adjustment mechanism. The device dc-gain is plotted in Fig. 4 as a function of V_b. Eq. 2 is fitted to the experimental data demonstrating the behavior of the system for different applied stiffness-adjustment voltages.

$$dc - gain = 0.0035(V_b + 1.8571)^2 + 10.788 \quad (2)$$

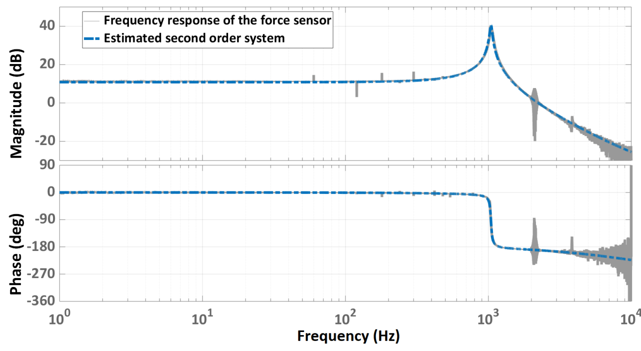

Fig. 2: Frequency response of the force sensor from its actuation input to the output of electrothermal displacement sensor and the estimated second-order model.

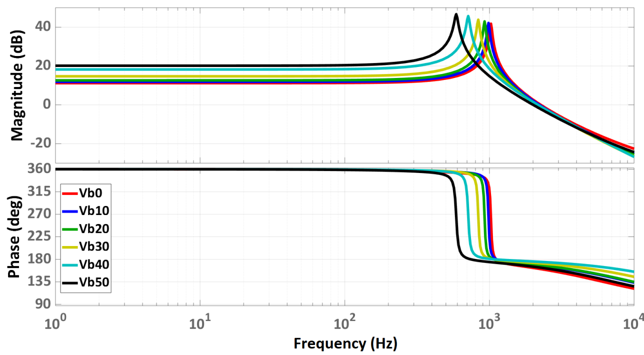

Fig. 3: Frequency responses of models fitted to the experimental data obtained from the force sensor for different stiffness adjustment voltages (V_b). The input is the voltage applied to the comb actuators and the output is the voltage measured at the electrothermal displacement sensor output for various stiffness adjustment voltages.

III. Control design

The force sensor's main control objective is to keep the stage at zero-displacement position, while measuring the applied external force. A closed-loop feedback mechanism is implemented to accomplish this. The system is schematically shown in Fig. 1.

A. Integral controller

The mechanical displacement of the MEMS force sensor can be nullified using a feedback control loop. As a result, the output of the force sensor will not be impacted by the nonlinearity brought on by the deflection of the mechanical flexures. Sensor-based feedback with integral action is one of the most common tracking methods in control systems. This is a simple controller, robust to modeling errors, and the large loop gain at low frequencies addresses sensor non-linearities. To follow the zero-displacement reference, the outer feedback loop contains the integral controller:

$$C_2 = \frac{k_i}{s} \tag{3}$$

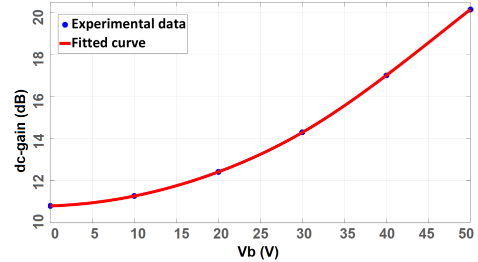

Fig. 4: Variation of the force sensor dc-gain with respect to the stiffness-adjustment voltage (V_b).

MATLAB PID Tuner is used to obtain the gain k_i by examining the system response and optimizing the speed and overshoot. This gain is adjusted to 1200. However, the bandwidth of integral tracking controllers is limited by the presence of resonant modes. The cause of such a limited closed-loop bandwidth can be explained by examining the loop gain $C_2G(s)$. The factor limiting the maximum feedback gain and closed-loop bandwidth is the gain margin. Damping control is an effective way to overcome the bandwidth constraints produced by mechanical resonance.

B. Resonant Controller

Additional damping can be augmented to the force sensor using a damping feedback loop. Increasing the damping ratio enables a corresponding increase in the closed-loop bandwidth and feedback gain [23]. Resonant controllers are easy to implement and provide guaranteed closed-loop stability when used on a collocated system [24]. Additionally, damping controllers offer a greater external disturbance rejection since they damp the mechanical resonance and eliminate the effect of unwanted disturbances on the system. However, these controllers cannot expand the closed-loop bandwidth above the resonance frequency on their own. The system's first resonant mode is effectively attenuated by the inner feedback loop using a resonant controller C_1 with the transfer function:

$$C_1 = \frac{1.7s^2}{s^2 + 142.6(2\zeta\omega_n)s + 1.45w_n^2} \tag{4}$$

ζ and w_n are the damping ratio and the first natural frequency of the nominal plant, respectively. Here, the controller parameters are chosen through inspection and tuned based on the system response to achieve the desired closed-loop response, gain and phase margins. The gain of C_1 is selected using the root locus of the feedback loop to maximize the closed-loop damping. Resonant controller's high-pass nature, minimizes the effect of flicker noise on the closed-loop system.

C. Controller performance

As soon as the force sensor comes into contact with the sample, its stiffness increases due to the mechanical contact. As a result, its resonant frequency increases and its dc-gain drops. This change becomes more noticeable as the force sensor is pushed towards the sample. In order to look into

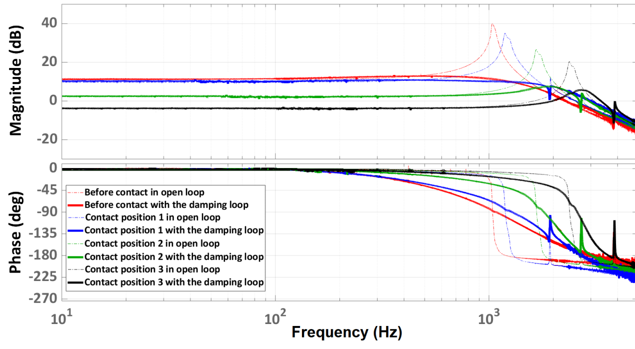

Fig. 5: Performance of the resonant controller over a wide range of frequencies and for various contact force values before and after contact.

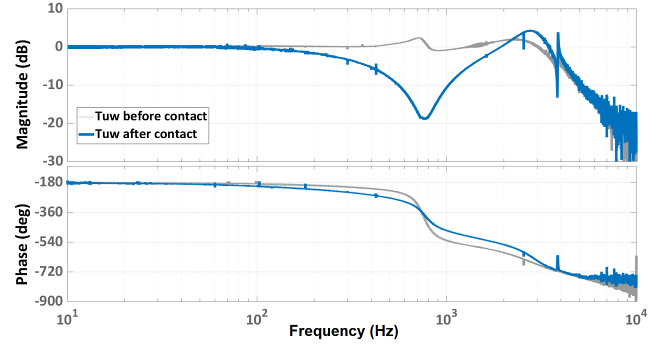

Fig. 6: Bode diagram of the force tracking transfer function (T_{uw}) before and after initial contact.

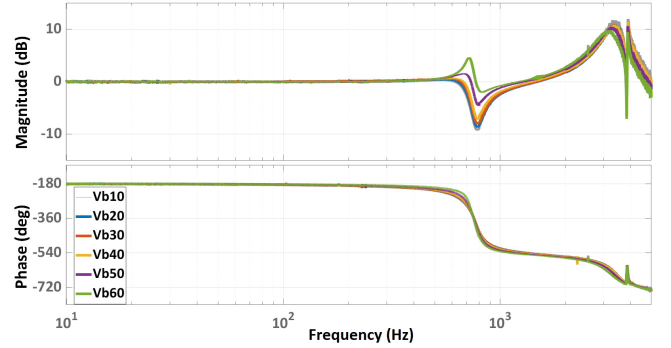

Fig. 7: The effect of applying different stiffness adjustment voltages along with a proper cascaded gain on the force tracking bandwidth after contact.

this phenomenon, an initial contact between the sensor and the cantilever is made and the frequency response of the coupled system from the input voltage applied to the electrostatic actuator to the output of the electrothermal displacement sensor is acquired. Fig. 5 compares the force sensor's primary response (without contact) with the system response after making contact in both open-loop and closed-loop cases. It can be noticed that the difference between the resonance magnitude and dc-gain reduces from 29.3 dB to 24.79 dB as a result of the mechanical contact. In order to investigate the controllers' effectiveness, first the damping controller is applied and the closed-loop frequency response of the system is measured at four different contact positions with and without the damping controller. The resonant controller works properly over a wide range of frequencies which demonstrates the robustness of the closed-loop system. Closing the second loop with an integrator adds additional roll-off to the system response.

IV. Force Tracking bandwidth

As we discussed in the previous section, the dynamics of the force sensor are altered when the sample stiffness is comparable to that of the force sensor's. In order to operate in closed loop, the controller parameters must be adjusted properly. Our main concern is the system gain since the resonant controller is designed to damp the resonant frequency over a wide frequency range as shown in Fig. 5. To restore the system dynamics to its pre-contact state, we must estimate the new dynamics. To accomplish this, after initial contact, we apply a small-amplitude, low-frequency load to the control signal and record the sensor output. Comparing the measured response to the nominal system response under the same load, we can obtain the new dc-gain and the amount needed to modify the gain. Based on the results of each experiment, we modify the system response using the stiffness adjustment mechanism (Eq. 2) as long as V_b is less than 50 V. If further improvement is needed, we use the cascaded gain to adjust the remaining gain difference. In the current experiment, an AFM probe with a stiffness of 27 N/m is used, which is comparable to the force sensor's stiffness (25.4 N/m). After contact, the zero-displacement tracking bandwidth drops from 340 Hz to 54.9 Hz and the dc-gain decreases from 10.8 dB to -4.32 dB. The transfer function from the input disturbance (w) to the output of the controller (u) is:

$$T_{uw}(s) = \frac{-\alpha G(C_1(s) + C_2(s))}{1 + \alpha G(C_1(s) + C_2(s))} \tag{5}$$

The force measurement bandwidth of the device is defined as the -3 dB point of the T_{uw} and has been experimentally determined for all stiffness adjusting voltages. Based on the results shown in Fig. 6, the tracking bandwidth of the closed-loop system before making contact with the sample is 3.47 kHz, but it drops to 290 Hz after contact. The stiffness adjustment mechanism is able to increase the dc-gain of the nominal system up to 9.4 dB, so the remaining difference can be tuned using gain adjustment. In this experiment, we apply a 50 V stiffness adjustment voltage which increases the dc-gain of the perturbed system to 5.07 dB. The remaining difference is made up with increasing the cascaded gain (α in Fig. 1) to 1.93. Knowing that various samples result in different outcomes, the force tracking bandwidth of the system has been increased to 766 Hz with gain adjustment. Fig. 7 illustrates the effect of gain adjustment on the transfer function between the external force (w) and the actuation signal (u) by applying various stiffness adjustment voltages to modify

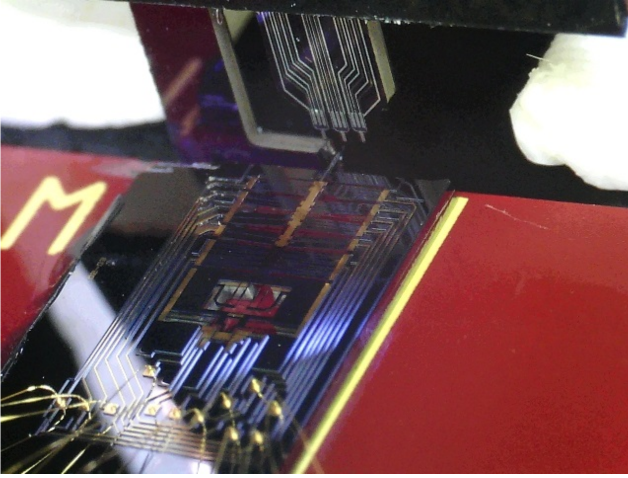

Fig. 8: Image of a MEMS force sensor wire bonded to a PCB and properly positioned using a 3-axis positioning stage, allowing the force to reach the sample.

the stiffness of the system along with a proper cascaded gain to adjust the remaining gain difference. Clearly, the tracking bandwidth has been modified significantly.

The results of the force tracking for sinusoidal, triangular and pulse inputs in time domain are discussed in the next section.

V. Experimental results

In order to investigate the force sensor's performance in closed loop, an experimental testbed is constructed as shown in figure Fig. 8. In this experiment, the controller output (u) and the probe displacement are both being tracked simultaneously. Performance of the proposed controllers are evaluated against sine, pulse and triangular inputs in Figures 9- 11 for different frequencies up to 500 Hz.

An important observation is that force tracking has been improved significantly by adjusting the loop gain after making contact. Note that the external force and control output are in volts and should be converted to force in newtons using the force calibration equation reported in [21]:

$$F_{act} = 1.9026 \times 10^{-10} v_a^2 + 9.2033 \times 10^{-6} v_a \qquad (6)$$

where F is in N and v_a is in V.

To quantify sensor's displacement measurement resolution, sensor noise is recorded in time domain with the sampling rate of 50 kHz for 50s using a dSPACE MicroLabBox. After subtracting the mean value of the noise data, the sensor's 1σ-resolution is computed as the root mean square (RMS) of the noise signal. By converting the noise RMS to displacement using the electrothermal sensor's calibration factor (1.9 μm/V), the 1σ-resolution of the sensor is obtained to be 3.74 nm.

The force measurement resolution is also calculated using the control signal generated by the controllers. The noise signal is recorded over a 10s time period, which is then converted to force using Eq. 6. The highest RMS of the force tracking resolution is measured to be 10.12 nN in closed loop. It should be noted that the closed-loop noise is recorded in an isolated box, whereas, the stiffness test is carried out in a normal laboratory environment.

Based on the experimental results, with the proposed controllers, the force sensor remains in the null position throughout a wide frequency range when subjected to pulse forces. It is also evident that as the frequency of the applied force increases, the reference tracking becomes less accurate. As shown in Fig. 10, the zero-displacement tracking error under sine loads is 10 nm, 58 nm, 115 nm, and 185 nm for 10 Hz, 50 Hz, 100 Hz, and 500 Hz, respectively. In Fig. 11, the zero-displacement tracking error for the triangular loads is 7 nm, 38 nm, 72 nm, and 120 nm for 10 Hz, 50 Hz, 100 Hz, and 500 Hz, respectively. Figures 9- 11 show that the force-tracking has been modified significantly, and dynamic forces with the frequency of up to 500 Hz can be measured with high precision. The system under high-frequency forces exhibit a small phase lag, which is negligible since the amplitude of the external force is of interest.

VI. Conclusion

The proposed MEMS force sensor is well suited for many micro and nano scale force measurements due to its small size, fine sensitivity, and ability to measure high-frequency dynamic forces. According to the characterization results, the device has a resonant frequency of 1050 Hz. It can be reduced to 592 Hz using the embedded stiffness-adjustment mechanism, where the dc-gain increases from 10.8 dB to 20.2 dB. The force sensing system is used to conduct experiments with an arbitrary sample to determine external forces. To accomplish this, we developed a null-displacement force sensing method to reduce the dependency of the measured force on changes in system dynamics. The control system consists of a resonant controller in the inner feedback loop combined with an integrator in the outer loop for reference tracking. In closed loop, the force measurement resolution of 10.12 nN in a range of $\pm$200 μN is obtained. To address the issue of changing system dynamics while interacting with the sample, we proposed a method in which, after initial contact, we apply a small-amplitude, low-frequency input to the system and record the sensor output to obtain the new system dynamics and tune the controllers accordingly, reducing the risk of damaging the sample and/or the force sensor. Simulations and experimental results validate the effectiveness of the proposed tracking and damping controllers. Compared to previous designs and control approaches, the proposed method improved the null-displacement and force tracking bandwidth, reaching 766 Hz for a sample with a stiffness comparable to the force sensor. The same method can be used on any sample with various stiffness.

References

[1] W. H. Wright, G. Sonek, Y. Tadir, and M. W. Berns, "Laser trapping in cell biology," *IEEE Journal of Quantum electronics*, vol. 26, no. 12, pp. 2148–2157, 1990.

[2] Y. Sun and B. J. Nelson, "Mems for cellular force measurements and molecular detection," *International Journal of Information Acquisition*, vol. 1, no. 01, pp. 23–32, 2004.

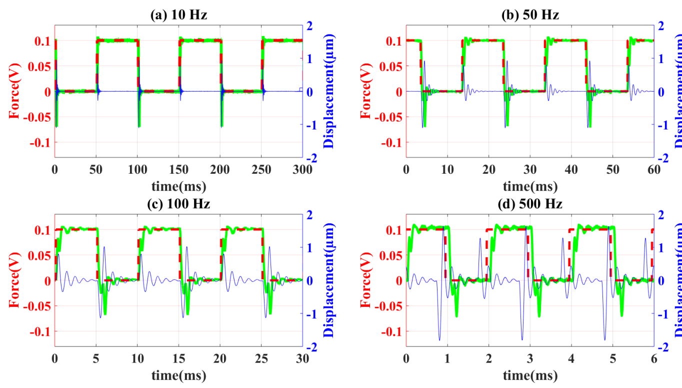

Fig. 9: Force sensing performance of the device to pulse inputs in contact with the cantilever. The left-hand scale is for external force (- -) and measured force (-) in volts, and the right-hand scale is the stage displacement (-) in micrometer.

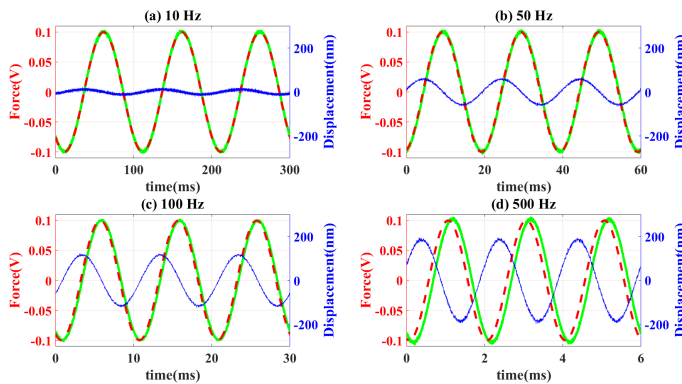

Fig. 10: Force sensing performance of the device after making contact with the cantilever using integral controller to sinusoidal inputs. The left-hand scale is for external force (- -) and measured force (-) in volts, and the right-hand scale is the stage displacement (-) in nanometer.

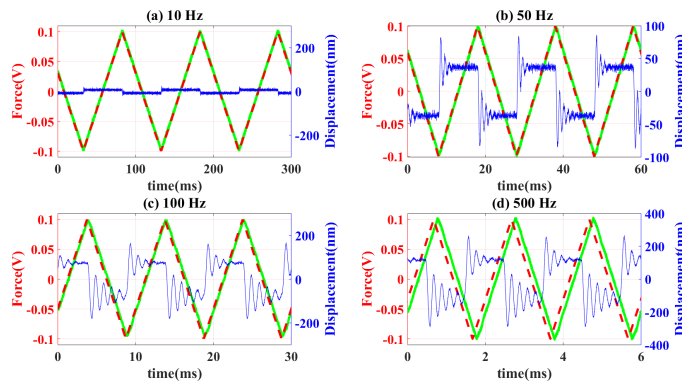

Fig. 11: Force sensing performance of the device after making contact with the cantilever using integral controller to triangular inputs. The left-hand scale is for external force (- -) and measured force (-) in volts, and the right-hand scale is the stage displacement (-) in nanometer.

[3] R. Bogue, "Recent developments in mems sensors: A review of applications, markets and technologies," *Sensor Review*, 2013.

[4] H. Park, N. Thanh-Vinh, K. Hirayama, T. Tsukagoshi, K. Noda, T. Takahata, K. Matsumoto, and I. Shimoyama, "Measuring the vibration of cells subjected to ultrasound using a mems-based force sensor array," in *2016 IEEE 29th International Conference on Micro Electro Mechanical Systems (MEMS)*, pp. 695–697, IEEE, 2016.

[5] Y. Sun and B. J. Nelson, "Biological cell injection using an autonomous microrobotic system," *The International Journal of Robotics Research*, vol. 21, no. 10-11, pp. 861–868, 2002.

[6] D. P. Allison, N. P. Mortensen, C. J. Sullivan, and M. J. Doktycz, "Atomic force microscopy of biological samples," *Wiley Interdisciplinary Reviews: Nanomedicine and Nanobiotechnology*, vol. 2, no. 6, pp. 618–634, 2010.

[7] I. Safenkova, A. Zherdev, and B. Dzantiev, "Application of atomic force microscopy for characteristics of single intermolecular interactions," *Biochemistry (Moscow)*, vol. 77, no. 13, pp. 1536–1552, 2012.

[8] D. Wang, S. Fujinami, K. Nakajima, S. Inukai, H. Ueki, A. Magario, T. Noguchi, M. Endo, and T. Nishi, "Visualization of nanomechanical mapping on polymer nanocomposites by afm force measurement," *Polymer*, vol. 51, no. 12, pp. 2455–2459, 2010.

[9] H. Janovjak, J. Struckmeier, and D. J. Müller, "Hydrodynamic effects in fast afm single-molecule force measurements," *European Biophysics Journal*, vol. 34, no. 1, pp. 91–96, 2005.

[10] H. Mahmoodi Nasrabadi, M. Mahdavi, M. Soleymaniha, and S. O. R. Moheimani, "High resolution atomic force microscopy with an active piezoelectric microcantilever," *Review of Scientific Instruments*, vol. 93, no. 7, p. 073706, 2022.

[11] A. Alipour, E. L. Fowler, S. O. R. Moheimani, J. H. G. Owen, and J. N. Randall, "Atomic-resolution lithography with an on-chip scanning tunneling microscope," *Journal of Vacuum Science & Technology B*, vol. 40, no. 3, p. 030603, 2022.

[12] M. K. Mishra, V. Dubey, P. Mishra, and I. Khan, "Mems technology: A review," *J. Eng. Res. Rep*, vol. 4, no. 1, pp. 1–24, 2019.

[13] M. Maroufi, H. Alemansour, M. Bulut Coskun, and S. O. Reza Moheimani, "An adjustable-stiffness mems force sensor: Design, characterization, and control," *Mechatronics*, vol. 56, pp. 198–210, 2018.

[14] M. Haque and M. Saif, "Application of mems force sensors for in situ mechanical characterization of nano-scale thin films in sem and tem," *Sensors and Actuators A: Physical*, vol. 97, pp. 239–245, 2002.

[15] Y. Sun and B. J. Nelson, "Mems capacitive force sensors for cellular and flight biomechanics," *Biomedical Materials*, vol. 2, no. 1, p. S16, 2007.

[16] K. J. Rebello, "Applications of mems in surgery," *Proceedings of the IEEE*, vol. 92, no. 1, pp. 43–55, 2004.

[17] B. Piriyanont, A. G. Fowler, and S. O. R. Moheimani, "Force-controlled mems rotary microgripper," *Journal of Microelectromechanical Systems*, vol. 24, no. 4, pp. 1164–1172, 2015.

[18] B. D. Jensen, S. Mutlu, S. Miller, K. Kurabayashi, and J. J. Allen, "Shaped comb fingers for tailored electromechanical restoring force," *Journal of Microelectromechanical Systems*, vol. 12, no. 3, pp. 373–383, 2003.

[19] S. Adams, F. Bertsch, K. Shaw, P. Hartwell, F. Moon, and N. MacDonald, "Capacitance based tunable resonators," *Journal of Micromechanics and Microengineering*, vol. 8, no. 1, p. 15, 1998.

[20] C. Mueller-Falcke, Y.-A. Song, and S.-G. Kim, "Tunable stiffness scanning microscope probe," in *Optomechatronic Micro/Nano Components, Devices, and Systems*, vol. 5604, pp. 31–37, SPIE, 2004.

[21] M. Maroufi, H. Alemansour, and S. O. R. Moheimani, "A high dynamic range closed-loop stiffness-adjustable mems force sensor," *Journal of Microelectromechanical Systems*, vol. 29, no. 3, pp. 397–407, 2020.

[22] M. Soleymaniha, M. B. Coskun, H. Mahmoodi Nasrabadi, A. Alipour, and S. O. R. Moheimani, "Design, fabrication and characterization of active atomic force microscope cantilever arrays," in *2021 IEEE 34th International Conference on Micro Electro Mechanical Systems (MEMS)*, pp. 883–886, 2021.

[23] A. J. Fleming, "Nanopositioning system with force feedback for high-performance tracking and vibration control," *IEEE/Asme Transactions on Mechatronics*, vol. 15, no. 3, pp. 433–447, 2009.

[24] S. O. R. Moheimani and B. Vautier, "Resonant control of structural vibration using charge-driven piezoelectric actuators," *IEEE Transactions on Control Systems Technology*, vol. 13, no. 6, pp. 1021–1035, 2005.